ACS OMEGA

Open Access

http://pubs.acs.org/journal/acsodf

Article

Comprehensive Understanding of the Heavy Oil Combustion Process: Reaction Behavior, Kinetic Triplet, and Mechanism Implication

Hong Yin, Ziqiang Chen, Yafei Chen,* Hua Tan, Mingyuan Wang, Donglin He, Ping Ouyang, and Haifeng Gong

Cite This: *ACS Omega* 2024, 9, 21164−21173

Read Online

ACCESS | Metrics & More | Article Recommendations | Supporting Information

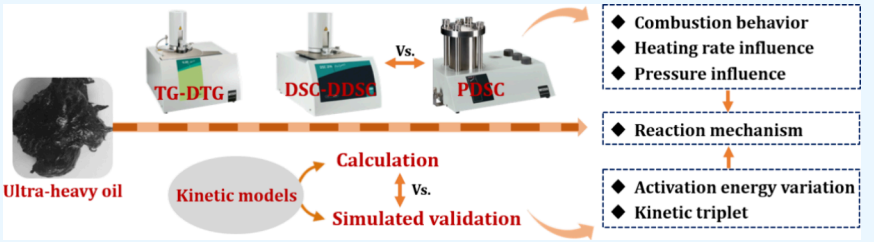

ABSTRACT: In this work, thermo-oxidative behavior, kinetic triplet, and free radical mechanism of ultraheavy oil during an in situ combustion (ISC) process were systematically surveyed via multiple thermal analysis techniques (TG/DTG/DSC/PDSC), model-free methods, and related mathematical simulation. First, specific mass loss, exothermic intensity, and corresponding temperature intervals were respectively determined in low-/high-temperature oxidation (LTO/HTO) regions. In addition, the comparison of atmospheric/pressurized differential scanning calorimetry (DSC/PDSC) experiments indicated that the pressurized conditions could obviously strengthen the oxidation progress with more heat emission. Then two model-free methods were contrastively employed for PDSC data to calculate LTO and HTO activation energy variations with the conversion rate. Moreover, the acceleratory rate model for LTO and the Sestak−Berggren model for HTO were accordingly picked as the most probable mechanism functions, which were later used to determine the simulated curves. Then, the simulations of $\alpha-T$ and $d\alpha/dT-T$ curves were respectively attained using Friedman equation in MATLAB software and contrasted with experimental data to validate the accuracy of the yielded kinetic triplet and forecast the combustion behavior. Further, the evolution pathways of the underlying oxidation mechanism was illustrated. This study updates the understanding of the nonisothermal combustion process, contributing to the subsequent numerical simulation and feasible investigation for in situ combustion implementation to enhance heavy oil recovery.

1. INTRODUCTION

One of the urgent and real issues in the world is the growing exhaustion of conventional petroleum resources and the fragility and inferiority of renewable energy deployment. In this situation, the contradiction between energy supply and demand could be alleviated via the exploitation of unconventional oil sources, such as heavy oil, bitumen, and tight oil, which account for over 70% of the remaining petroleum resources all over the world.[1,2] Therein, in situ combustion (ISC) is deemed as a valuable and promising thermal technique to improve the recovery of inferior oils, during which complicated oxidation reactions are undergone to generate the combustion front with enormous heat to improve the heavy oil viscosity and quality.[3−5]

Since the early 1950s, over 300 ISC field tests and commercial operations have been carried out worldwide, during which several representative cases were Suplacu de Barcau (Rumania), Balol (India), and Bellevue (U.S.) oilfields.[6] Besides the reservoir feature, engineering parameter, and factitiousness operation, the ambiguous and inadequate understanding of potential oxidation process for a specific oil reservoir was an important reason for many failure cases, which played a decisive role in coke intensity and quality, ignition timing, and combustion front adjustment.[5,7,8] Therefore, it was fundamental and indispensable for laboratory experiments to characterize specific details of the oxidation behavior and kinetic mechanism, which could provide prerequisite screening and understanding for subsequent numerical simulations and field tests.

Various thermal analysis techniques have been widely accepted and employed to interpret the thermal (pyrolysis and

Received: February 1, 2024
Revised: April 12, 2024
Accepted: April 23, 2024
Published: May 1, 2024

oxidation) characteristics of crude oils under isothermal and nonisothermal conditions, which could provide specific or general information on thermal reaction behaviors and kinetics and have been reported in numerous studies.[9−11]

Kök briefly reviewed the application of principal thermoanalytical methods, including thermogravimetry (TG), differential thermal analysis (DTA), and differential scanning calorimetry (DSC), to characterize fossil fuel kinetics, and it was indicated that these methods presented a significant improvement in specific determinations of pyrolysis and oxidation behaviors, particle size and heating rate effects, calorific value influences, and kinetics during the thermal process.[10] Furthermore, Khoshooei et al. comprehensively studied the application of DSC and relative thermal analysis methods to petroleum-based products, including the statuses, limitations, and recommendations.[9] In consideration of the pressurized and near-adiabatic conditions for actual reservoirs, conventional thermal analysis methods could not accurately reflect underground reaction situations, while more and more attention has been paid to emerging methods to determine the kinetics under pressurized conditions, such as an accelerating rate calorimeter (ARC),[12] a pressurized differential scanning calorimeter (PDSC),[13] and ramped-temperature oxidation (RTO).[14] Therein, the heat release rate for high-temperature oxidation (HTO) with dramatic reactions usually exceeded the upper limitation of the ARC tracking surveillance, which affected the integrity and validity of experimental data.[15]

In addition to oxidation behavior characterization, the interpretation of kinetic characteristics and corresponding computation of parameters were another emphasis for the thermal analysis study, which was closely associated with kinetic approach selection. Under the nonisothermal condition, there have been two widely adopted kinetic approaches, model-free and model-fitting methods.[11,16,17] For the model-fitting method, Arrhenius, Coats−Redfern, and Ingraham−Marrier equations were typical representations based on Arrhenius theory and single heating-rate pattern to acquire kinetic parameters.[18] Aiming to eliminate the impact of heating rates and the deviation of hypothetical reaction models, the model-free method has received wide attention and recommendation, which could be further subdivided into differential and integral forms.[11,16] Besides, some derived methods, such as the Popescu method,[19] have been gradually adopted to reduce the error caused by the approximate solution of temperature integration. A main motivation and target of the kinetic study was to predict the corresponding thermal behavior and provide fundamental information for subsequent numerical simulation and candidate screening, via which the reactivity and thermal characteristic of a given oil sample in an untested environment could be determined.

Based on the above analysis, TG-DTG/DSC-DDSC/PDSC data under different heating rates were respectively obtained to comprehensively evaluate the corresponding nonisothermal oxidation behavior, heating rate influence, and pressure effect for the ultraheavy oil in this study. Then the differential (Friedman) and integral (distribution activation energy model, DAEM) equations of the mode-free method were contrastively employed to process the PDSC data to confirm the activation energy (E) distribution and frequency factor (A), owing to their being more realistic for PDSC data rather than TG/DSC data. Besides, an advanced approach, propounded by Shahcheraghi et al.,[20] was engaged for PDSC data to determine the most probable mechanism function, $f(\alpha)$. One should clearly understand that no matter which reaction model determined method is adopted, more attention should be paid to identifying the most probable mechanism functions rather than the underlying "true reaction model". Further, the contrast of experimental and simulated conversion ($\alpha-T$) and conversion variation ($d\alpha/dT-T$) curves was analyzed to verify the accuracy and applicability of yielded kinetic triplets that should be adequate to parametrize the oxidation behavior at any chosen temperature and/or conversion extent. Finally, the underlying oxidation mechanism was illustrated via the elucidation of the free radical reactions with main evolution pathways. The knowledge obtained from this work could update the understanding of the heavy oil oxidation process and provide crucial information for subsequent numerical modeling and feasible investigation of the ISC technique to enhance oil recovery.

2. MATERIALS AND METHODS

2.1. Materials. The original material (ultraheavy crude oil) in this study was from the Northwest Bureau of Sinopec, China. Before the experiments, the oil sample underwent dehydration and impurity removal procedures. Then the corresponding carbon, hydrogen, sulfur, nitrogen, and oxygen contents were analyzed by using an elemental analyzer (Elementar Vario). As for the four components (SARA) and density, an analysis method (SY/T5119-2016) and densimeter (Anton Paar DMA) were respectively adopted, specific procedures for which have been presented in previous studies.[7,21] And these physiochemical characteristics are shown in Table S1 in the Supporting Information.

2.2. Experimental Apparatus and Procedures. According to the literature, thermal behaviors, kinetics, thermodynamic parameters, and oxidation evolution pathway of the ultraheavy oil during ISC process can be effectively characterized by thermal analysis experiments (TG-DTG/DSC-DDSC/PDSC), model-free (Friedman, DAEM, and Shahcheraghi) kinetic approaches, and thermodynamic theory, respectively.

2.2.1. Thermal Analysis Experiments. 2.2.1.1. Thermogravimetric Analysis (TG-DTG). Thermogravimetric experiments for targeted crude oil were realized on a NETZSCH 209 F3 Tarsus thermogravimetric analyzer with three heating rates (6, 9, and 12 °C/min). Besides, a nonisothermal oxidation atmosphere was maintained by an injected air flow (50 mL/min) during the whole process (30−700 °C). To eliminate the influence of mass transfer, the weight of the sample in each experiment was less than 10.0 mg and the sample preparation was based on an ASTM standard (D2013-72).[19,22] Before the experiments, both calcium oxalate monohydrate and silver were considered separately for temperature calibration and buoyancy effect determination.

2.2.1.2. Differential Scanning Calorimetry Analysis (DSC-DDSC). Differential scanning calorimetry analysis experiments were accomplished via a NETZSCH 214 Polyma calorimeter. The experiments were conducted under an air atmosphere (50 mL/min) from 30 to 700 °C with constant heating rates (6, 9, and 12 °C/min). For the DSC system, sapphire and indium were employed to calibrate the cell and temperature modules before each experiment. Similar to TG-DTG experiments, the ASTM standard acted as the guideline to prepare the sample (∼10.0 mg) for each experiment.[7,22] Based on DSC data, the corresponding first-order differential curve (DDSC) could be determined to describe the varied heat flow tendency, as reported in previous literature.[5,11]

https://doi.org/10.1021/acsomega.4c01032
ACS Omega 2024, 9, 21164−21173

Table 1. Mathematical Expressions of Functions Sh(α) for the Well-Known Reaction Functions

model	symbol	$f(\alpha)$	Sh(α)
acceleratory rate equations	P_n ($n \neq 1$)	$(1/n)\alpha^{(1-n)}$	$(1-n)/\alpha$
Avrami−Erofeev	A_n	$n(1-\alpha)[-\ln(1-\alpha)]^{(1-1/n)}$	$[1-(1/n)+\ln(1-\alpha)][(\alpha-1)\ln(1-\alpha)]^{-1}$
diffusion mechanism	D_1	$(1/2)\alpha^{-1}$	$-1/\alpha$
	D_2	$[-\ln(1-\alpha)]^{-1}$	$[1/(1-\alpha)]/\ln(1-\alpha)$
	D_3	$[(3/2)(1-\alpha)^{2/3}][1-(1-\alpha)^{1/3}]^{-1}$	$-(2/3)(1-\alpha)^{-1}[1+(1/2)(1-\alpha)^{1/3}(1-(1-\alpha)^{1/3})^{-1}]$
	D_4	$(3/2)[(1-\alpha)^{-1/3}-1]^{-1}$	$(1/3)(1-\alpha)^{-4/3}[(1-\alpha)^{-1/3}-1]^{-1}$
phased boundary reaction	R_1	constant	0
	R_2	$2(1-\alpha)^{1/2}$	$(1/2)(1-\alpha)^{-1}$
	R_3	$3(1-\alpha)^{2/3}$	$(2/3)(1-\alpha)^{-1}$
chemical process	F_n ($n \neq 0, 1/2, 1/3, 1$)	$(1-\alpha)n/\lvert 1-n\rvert$	$-n/(1-\alpha)$
autocatalytic model	SB(m,n)	$\alpha^m(1-\alpha)^n$	$(m/\alpha)-(n/(1-\alpha))$

2.2.1.3. Pressurized Differential Scanning Calorimetry Analysis (PDSC). PDSC trials were performed using a NETZSCH DSC 204 HP Phoenix to investigate the heat flow variation of nonisothermal oxidation at an atmospheric pressure of 5.0 MPa with different heating rates (6, 9, and 12 °C/min), which approximated the actual reservoir pressure. For the PDSC cell, a spring-action purge valve was connected to the exhalation line to retain the fixed pressure. Before each experiment, the PDSC system was calibrated based on references, and the oil sample (∼1.0 mg) was put in the reactor with a reaction interval of room temperature to 600 °C.[23,24]

2.2.2. Kinetic Triplet Study. As a complex mixture of enormous hydrocarbons and nonhydrocarbons, the ultraheavy crude oil also followed the kinetic theory and corresponding mechanism during thermal analysis experiments. In the development of kinetic theory, in the late 1800s both Arrhenius and van't Hoff proposed that the rate constant, k, was very closely related to the temperature, T, for the kinetic equation. Therein, it was widely used for the rate constant−temperature relationship (Arrhenius theory), which was derived based on the equilibrium constant−temperature relationship.[16,17]

$$k = A\exp(-E/RT) \tag{1}$$

In eq 1, the symbols A, E, R, and T respectively indicate the frequency factor, activation energy, molar gas constant, and thermodynamic temperature. For the homogeneous reaction, this equation was suitable to describe almost all of the elementary reactions and most complex reactions, which has also been widely adopted and acceptable for a heterogeneous system.[11,16]

For the nonisothermal situation with constant heating rate, the following expression could be derived, in which the conversation rate term was α, the heating rate term was β, and the mechanism function term was $f(\alpha)$.

$$\mathrm{d}\alpha/\mathrm{d}T = \frac{A}{\beta}\exp\left(-\frac{E}{RT}\right)f(\alpha) \tag{2}$$

On these grounds, the quantitative characterization process of the crude oil oxidation reaction, based on thermal analysis kinetics, could be transferred into the determination of the most probable mechanism function, activation energy, and frequency factor, which were followed for the reaction process and regarded as the kinetic triplet.[17,19,25] Then the corresponding reaction rate could be obtained to supply scientific guidance for the quantitative description and potential mechanism estimation of the crude oil oxidation process by utilizing experiments and simulations.

2.2.2.1. Pre-exponential Factor Determination. The frequency factor is defined as the proportion of valid collisions to total collisions based on collision theory. While, in transition state theory, it is connected with the entropy variation to form the transition state. In a word, the frequency factor, related to reaction temperature, could be expressed by the following:[26,27]

$$A = A_0 T^m \tag{3}$$

In eq 3, A_0 is a constant and independent of temperature, and m is an integer or half-integer not greater than 4. In this study, the frequency factor, A, could be ascertained via the intercept of the regression curves of $\ln(\beta/T^2)$ vs $1/T$ by the DAEM method.

2.2.2.2. Activation Energy Determination. For the activation energy dependence on reaction temperature, a combination of eqs 1 and 3 could derive the following expression, in which E_0 is a constant independent of temperature.

$$E = RT^2\frac{\mathrm{d}\ln k}{\mathrm{d}t} = E_0 + mRT \tag{4}$$

The intensity of activation energy variation, $mR\Delta T$, is dependent on the temperature change, ΔT. In order to improve calculation accuracy and reflect the activation energy variation with temperature, integral (DAEM) and differential (Friedman) forms of the model-free method were employed to ascertain the activation energy variation rather than the model-fitting method, which was consistent with the International Confederacy for Thermal Analysis and Calorimetry (ICTAC) committee's recommendation.[17,19]

As one of the least complicated and generally reasonable linear different model-free methods, the final expression of Friedman method is given as[16]

$$\ln\left(\beta\frac{\mathrm{d}\alpha}{\mathrm{d}T}\right) = \ln[Af(\alpha)] - E/RT \tag{5}$$

The DAEM method is an extensively applied model-free method assuming that several lateral, irrevocable, and first-order reactions with varying activation energies concurrently exist. Via several derivations, the DAEM equation can be demystified in this way:[11,16,23]

$$\ln(\beta/T^2) = \ln(AR/E) - 0.6075 - E/RT \tag{6}$$

For the given conversion with corresponding heating rates, the activation energy could be respectively ascertained via the linear regressions of $\ln(\beta\,\mathrm{d}\alpha/\mathrm{d}T)$ vs $1/T$ for the Friedman method and $\ln(\beta/T^2)$ vs $1/T$ for the DAEM method.

2.2.2.3. Reaction Model Determination. Attempts to study kinetic model functions began in the late 1920s, and relevant research rapidly developed in the 1930s and 1940s. Therein,

https://doi.org/10.1021/acsomega.4c01032
ACS Omega 2024, 9, 21164−21173

most of these kinetic model functions assumed that there was a local reactive active region at the interface between reactants and products in the solid-phase reaction. In addition, the reaction progress could be characterized via the advance of this interface and would be determined by the deduction of various key steps that controlled the reaction rate.

Shahcheraghi et al.[20,28] initiated an advanced reaction model calculation procedure based on an isoconversional analysis, which could precisely emulate both single-step and multistep kinetics and can be described as

$$\frac{f'(\alpha)}{f(\alpha)} = \mathrm{Sh}(\alpha) = \left(\frac{1}{\mathrm{d}\alpha/\mathrm{d}t}\right)\left[\frac{\mathrm{d}^2\alpha/\mathrm{d}t^2}{\mathrm{d}\alpha/\mathrm{d}t} - \frac{\beta}{E_\alpha}\frac{\mathrm{d}E_\alpha}{\mathrm{d}T} + \frac{2\beta}{T_\alpha}\right] \quad (7)$$

in which $\mathrm{Sh}(\alpha)$ is the ratio between differentiated and actual reaction models. It was evident that the utilization of experimental data could calculate the right-hand side, while the left-hand side could be determined via common theoretical reaction models, as shown in Table 1. When the theoretical curve presented the uppermost association to the experimental data, the corresponding reaction model could be picked as the most suitable mechanism function.

3. RESULTS AND DISCUSSION

3.1. Nonisothermal Combustion Behavior. *3.1.1. TG-DTG/DSC-DDSC Analysis.* Figure 1 reveals the TG-DTG curve

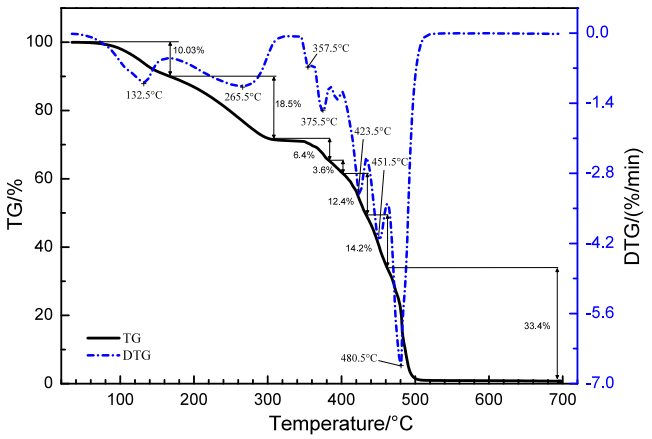

Figure 1. TG-DTG curve comparison for the ultraheavy oil at 6 °C/min.

of ultraheavy oil ramped-temperature oxidation with 6 °C/min. The broad and fluctuating trend in the DTG curve indicated a complicated oxidation process with continuous mass loss over a wide oxidation temperature range.

Specifically, the weak distillation phenomenon (<170 °C) and prominent oxidation addition reaction (170−358 °C) resulted in the first two slight peak valleys in the DTG curve, during which 29.85% mass loss in the TG curve corresponded to the distillation of residual water and partial light hydrocarbons, and the addition reactions of hydrocarbon fractions. With temperature increment, a series of complicated dehydrogenation, dealkylation, aromatization, and condensation reactions, indicated by obvious undulation in the DTG curve, were further triggered for low-temperature oxidation (LTO) products to coke deposition.[3,5] Then deposited coke underwent a drastic high-temperature oxidation (HTO), namely a combustion process, with great heat emission and the fastest mass loss rate in 480.5 °C. Besides, 49.43% of mass loss in the HTO stage, to some extent, indicated that the HTO process played a leading role. It is worth noting that the stepped decline for the DTG curve at the HTO early stage (451.5 °C) might be due to coke formation being intermingled with coke combustion to maintain a continuous coke supply until the sample exhaustion.

A combination of DSC and its first-order differential (DDSC) curves could provide a more intuitive understanding of specific exothermic behaviors,[5,11] as depicted in Figure 2. Generally, it

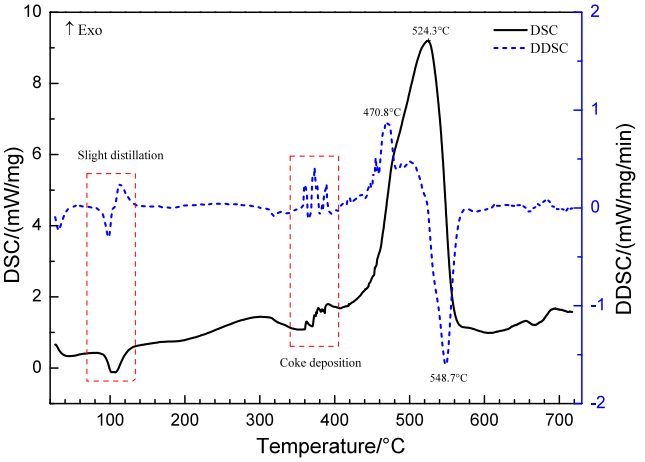

Figure 2. DSC-DDSC curve comparison of the ultraheavy oil at 6 °C/min.

was not easy to assign an obvious peak in the DSC curve to distinguish LTO and FD stages, while the related HTO peak (524.3 °C) was greatly distinctive. With the aid of the DDSC curve, the weak distillation and complicated coke deposition were distinctly identified, which was consistent with the TG-DTG analysis. In addition, the highest peak value of the DDSC curve at 470.8 °C indicated the fastest heat flow rate, while the fastest mass loss rate was observed at 480.5 °C. From such a perspective, it was indicated that a deviation existed between the mass loss and corresponding heat flow, which was attributed to oxidation reaction complexity and response hysteresis.

In order to evaluate heating rate influence, TG-DTG and DSC curves with 6, 9, and 12 °C/min are respectively exhibited in Figures S1 and S2 in the Supporting Information. With an increase in heating rate , corresponding fluctuations of TG/DTG/DSC curves were respectively toward higher temperatures with wider temperature intervals and higher peak values in each stage, as shown in Table 2.

The high heating rate led to a large temperature deviation between the surface and inner of sample particles, deteriorating the reaction progress and strengthening the inertia effect of devolatilization. Besides, more reactions were undergone in less time, and this led to more heat flow release. But total HTO heat enthalpy was relatively constant under similar peaks, which was in accord with the isoconversional principle.[29]

3.1.2. PDSC Analysis. Figure 3 illustrates the PDSC curve at 5 MPa and 6 °C/min to investigate the pressurized thermal flow variation, and the DSC curve is also presented as a reference.

Overall, two more prominent exothermic peaks (LTO at 252.0 °C, and HTO at 447.0 °C) were observed in the PDSC curve corresponding to lower threshold temperatures, smaller peak temperatures, higher peak values, and more heat release, as presented in Table S2. This was due to the fact that the

https://doi.org/10.1021/acsomega.4c01032
ACS Omega 2024, 9, 21164−21173

Table 2. Range, Peak Temperature, Mass Loss, and Peak Area of the Ultraheavy Oil

	LTO			FD		HTO			
heating rate (°C/min)	temperature range (°C)	peak temperature (°C)	mass loss (%)	temperature range (°C)	peak temperature/ (°C)	temperature range (°C)	peak temperature (°C)	mass loss (%)	peak area (kJ/g)
6.0	30−341	261.5	29.0	341−458	37.0	458−700	475.8	33.0	6.14
9.0	30−347	267.1	27.0	347−465	39.0	465−700	485.2	33.0	5.90
12.0	30−351	270.6	24.0	351−482	42.0	482−700	508.7	32.0	6.37

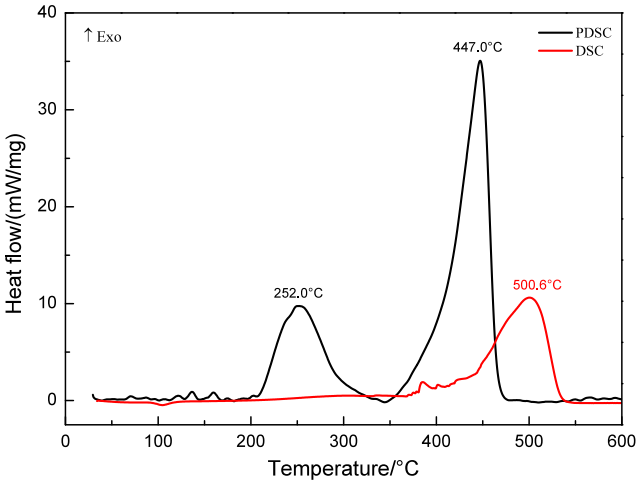

Figure 3. PDSC and DSC curve comparison for ultraheavy oil at 6 °C/min.

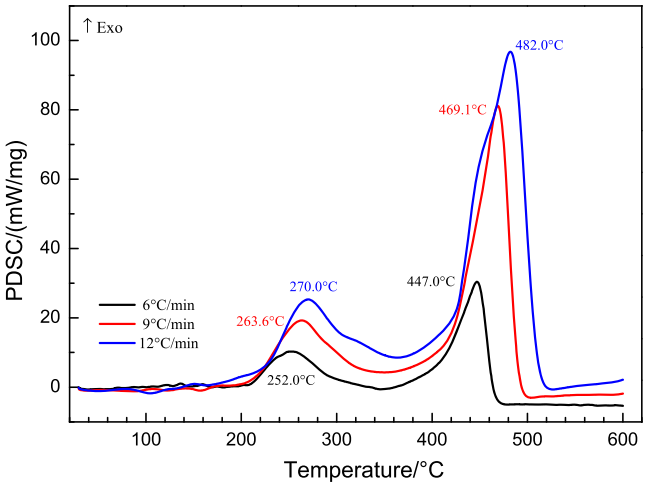

Figure 4. PDSC curves of ultraheavy oil at different heating rates.

pressurized condition could restrain the distillation process by an endothermic phenomenon and enhance the amount and quality of hydrocarbons to undergo exothermic oxidation reactions. Furthermore, the oxygen concentration in the oil phase was enriched under pressurized conditions, which facilitated oxidation progress with a higher exothermal flow compared with that in DSC curve.[13,24,30] In addition, the multiple increment (6.4×) in the LTO stage was extremely greater than that (2.1×) in the HTO stage for exothermic peak values. Thereby, the pressurized environment had a significant promoter action on the oxidation reaction and exothermic progress, especially in the LTO region. From this point of view, it provided a positive signal, and the possibility for a significant LTO exothermal increment under high-pressure reservoir conditions was easily available and could promote the stability of the combustion front in a lower temperature range.

Further, a comparison of PDSC curves is given in Figure 4. It was observed that a higher heating rate would shift the PDSC curve to the upper right with a higher threshold temperature and temperature interval, which was in step with the TG/DSC analysis. Particularly, for the heating rate increment from 6 to 12 °C/min, the LTO peak temperature shifted from 252.0 to 270.0 °C with a 1.46× increment of the peak value, while the corresponding HTO peak temperature increased from 447.0 to 482.0 °C with the peak heat flow increasing by 2.17×. It could be speculated that the high heating rate shortened the duration time of LTO and FD stages with worse coke deposition, and consequently the HTO exothermic peak was more sensitive to heating rate variation.

3.2. Combustion Kinetics. *3.2.1. Kinetic Parameter Calculation.* In order to more finely characterize the kinetic parameter variation, this study processed and divided PDSC data into LTO and HTO regions, and they were respectively incorporated into DAEM and Friedman methods to contrastively acquire kinetic parameters. After delegating specific temperature values under selected conversion degrees (0.05−0.98), Friedman and DAEM curves are respectively plotted in Figures 5 and 6 to obtain specific LTO and HTO kinetic parameters with relatively high correlation coefficients (R^2 > 0.930 for Friedman and R^2 > 0.952 for DAEM) and low standard deviations (r_{SD} < 0.421 for Friedman, and r_{SD} < 0.476 for DAEM), presenting a satisfactory linear fitting process. Besides, specific fitting results are respectively given in Tables S3 and S4.

In regard to specific LTO and HTO activation energies, the corresponding relationship between E and α could be determined, as illustrated in Figure 7. Generally, LTO and HTO average activation energies were respectively 109.4 and 180.9 kJ/mol for the DAEM method, while those values were respectively 74.7 and 135.7 kJ/mol via the Friedman method. This difference was mainly attributed to the variation of equation parameters, inaccuracy of numerical differentiation, and the premise from which those methods were derived.[16] In order to facilitate the follow-up analysis, the activation energy derived from the DAEM method was selected as an illustration to determine the latent oxidation mechanism. The LTO and HTO activation energy variations both presented a similar trend of an initially dramatic descent (0.05−0.15), then leading to a decline segment (0.15−0.90), and finally an obvious ascent (0.90−0.98).

Specifically, a high threshold energy (250 kJ/mol at α = 0.05) was required to trigger free radical chain reactions; then the accumulation of generated heat would gradually reduce energy demand and promote LTO progression with a decreasing trend of activation energy (α < 0.90). With oxidation addition reaction progress, previously oxidized products would further undergo dealkylation, aromatic condensation, and polycondensation reactions with higher energy demand, and the activation energy

https://doi.org/10.1021/acsomega.4c01032
ACS Omega 2024, 9, 21164−21173

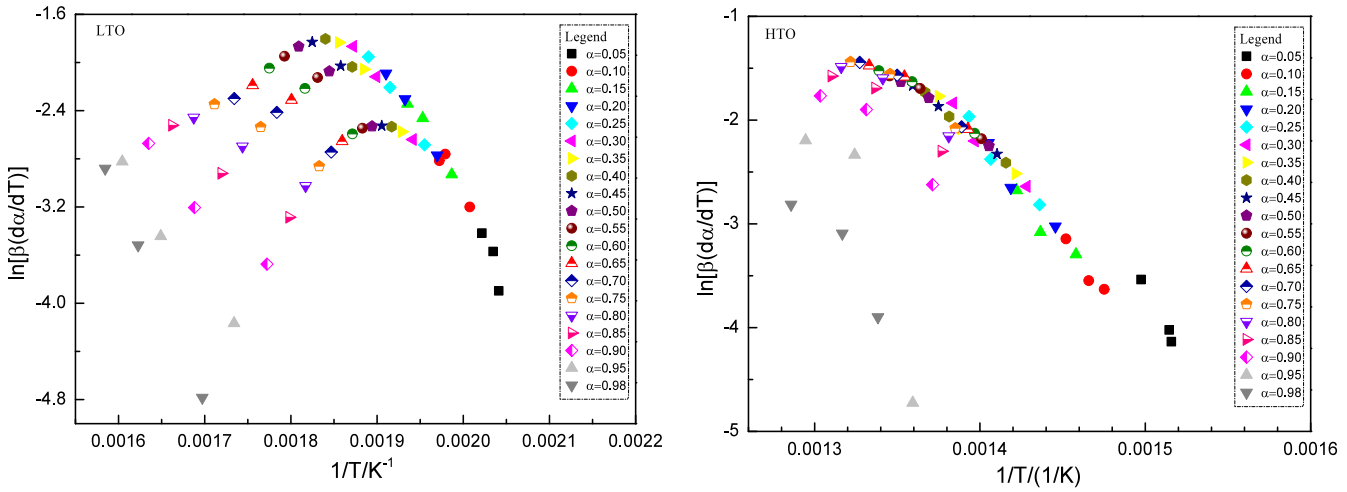

Figure 5. Kinetic curves of the ultraheavy oil at different conversion rates by the Friedman method.

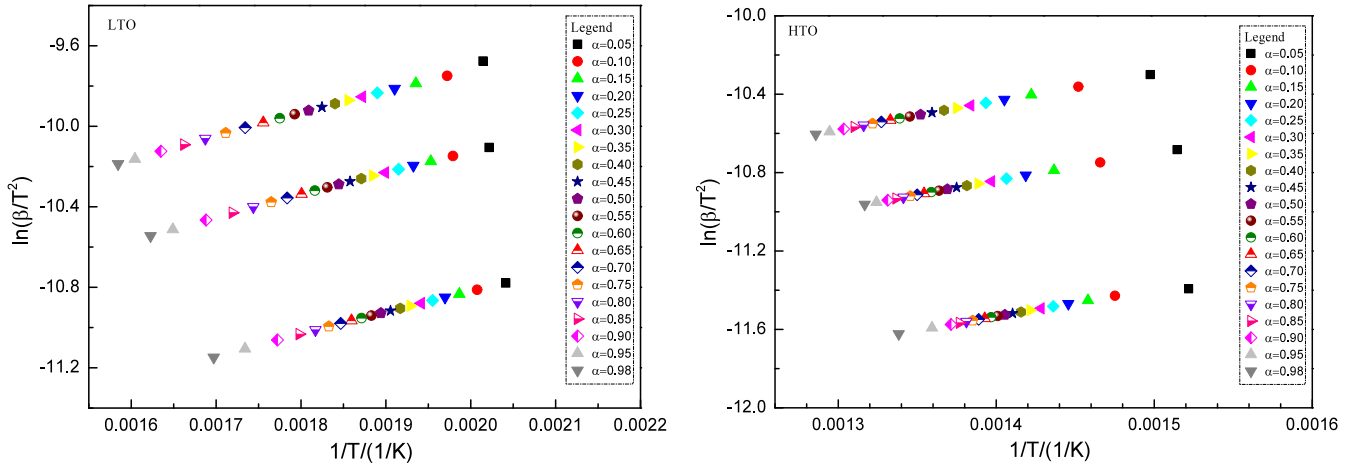

Figure 6. Kinetic curves of the ultraheavy oil at different conversion rates by the DAEM method.

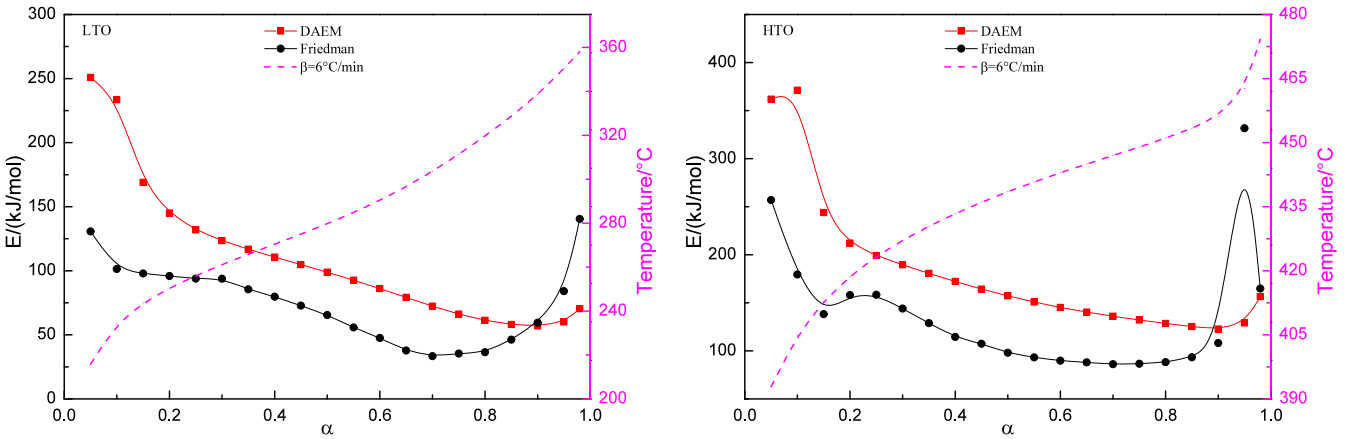

Figure 7. *E*-*α* curve comparison for the ultraheavy oil in LTO and HTO stages.

showed an evident uptrend. For the HTO process, the duration of coke generation in the initial period and the trigger of a combustion reaction corresponded to high activation energy ($\alpha < 0.15$). As the combustion process continued, the combustion of active coke would generate enormous heat with a distinct activation energy decrease ($0.15 < \alpha < 0.90$). In the late stage ($\alpha > 0.90$), coke shortage would gradually terminate the combustion reaction with decreasing heat generation and increasing activation energy demand.

The frequency factor can be calculated via eq 6, and its variation with conversion is shown in Figure 8. The fluctuation tendency of the frequency factor was equivalent to that of activation energy, indicating that there existed an internal relationship between E and A, namely, a kinetic compensation

https://doi.org/10.1021/acsomega.4c01032
ACS Omega 2024, 9, 21164−21173

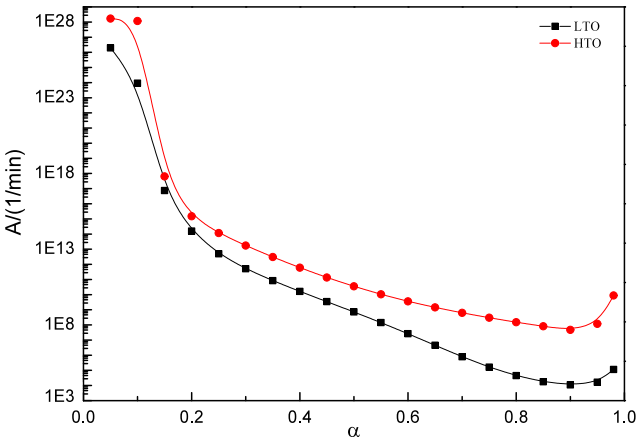

Figure 8. Frequency factor variation for ultraheavy oil in LTO and HTO stages.

effect, as shown in Figure 9. Regardless of LTO and HTO stages, a high activation energy corresponded to a high frequency factor,

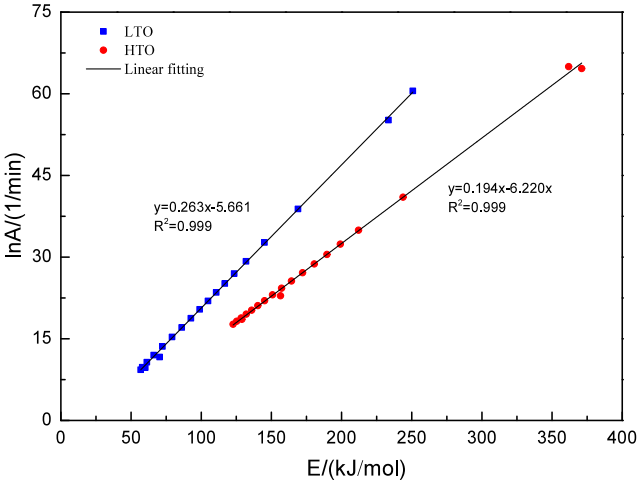

Figure 9. Relationship between ln A and E for ultraheavy oil in LTO and HTO stages.

while a low activation energy corresponded to a low frequency factor, which reflected a linear relation between ln A and E. Based on the transition state theory, it was actually affirmed that the relationship between activation entropy and activation enthalpy was bound up with the inherent property of the specific oil sample.

3.2.2. Kinetic Model Determination. In order to procure the most probable mechanism function, the experimental Sh(α) was evaluated from PDSC data (under 6 °C/min) in LTO and HTO stages, respectively, and then several theoretical Sh(α) curves were compared via MATLAB software to pick the best-fitted reaction model, as illustrated in Figure 10.

It was obviously witnessed that the LTO process of this ultraheavy oil followed the acceleratory rate model ($P_{-0.468}$), while the Sestak−Berggren (SB) model could describe the HTO stage with the specific parameters m = 0.649 and n = 0.886, during which a high reliability was presented for the chosen reaction models (R^2 = 0.919 for LTO, and R^2 = 0.953 for HTO). Furthermore, it was inferred that the nonisothermal oxidation for this ultraheavy oil was complicated and was depicted via the multistep reaction models.

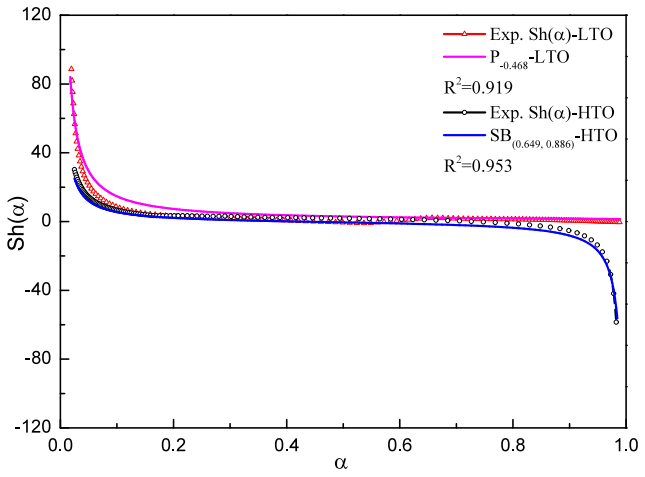

Figure 10. Experimental and theoretical Sh(α) curves in the LTO and HTO stages (6 °C/min).

3.2.3. Combustion Behavior Simulated Validation. Remarkably, no matter how many models were presented and selected in the tryout list, it was not enough to include and acquire a completely appropriate model. However, any unavoidably incomplete list of models would always produce one or several most probable mechanism functions as the reaction model.[19] Under this realistic circumstance, it was fundamental and indispensable to further check the reasonability and accuracy of the yielded kinetic triplet. Although little attention has been paid to it in present kinetic researches, it is crucial for this process to facilitate subsequent kinetic prediction, which is the most important practical utilization of a kinetic study to parametrize the thermal reaction process in regard to variables such as the temperature and conversion degree.[16]

Based on the yielded kinetic triplet, the simulative $\alpha-T$ and $d\alpha/dT-T$ curves could be respectively reconstructed via their substitution into eq 8. Meanwhile, a program coded in MATLAB was employed to acquire the result, which could be further used to predict the conversion rates under the extrapolated conditions.[31] Moreover, the residual sum of squares (RSS) was introduced to evaluate the difference between the experimental and simulated data, represented as

$$\mathrm{RSS} = \sum_{\alpha=0}^{1} (y_{\mathrm{exp}} - y_{\mathrm{model}})^2 \tag{8}$$

Figures 11 and 12 respectively present the comparison of $\alpha-T$ and $d\alpha/dT-T$ curves, and the corresponding residual variations between experimental and simulated data were respectively are shown in Figures S3 and S4. Visually, it could be seen that both simulated curves were highly related to the experimental data, especially for the LTO and HTO principal parts. Besides, there were some deviations for the $d\alpha/dT-T$ curve in 140−165 °C, which might be ascribed to the slight distillation process. As for the fluctuations in initial and final periods for HTO $\alpha-T$ and $d\alpha/dT-T$ curves, the complicated thermal cracking for coke deposition and the unstable combustion at the beginning and end might be the potential causes.

Based on the residual variation, obtained RSS values in $\alpha-T$ curves were respectively 2.8×10^{-3}, 2.4×10^{-3}, and 7.7×10^{-3} for the LTO stage and 2.8×10^{-2}, 2.2×10^{-2}, and 5.8×10^{-3} for the HTO stage, while the RSS values for $d\alpha/dT-T$ curves were respectively 1.86×10^{-5}, 4.74×10^{-6}, and 2.91×10^{-5} for LTO and 2.12×10^{-5}, 4.33×10^{-5}, and 3.75×10^{-6} for HTO

https://doi.org/10.1021/acsomega.4c01032
ACS Omega 2024, 9, 21164−21173

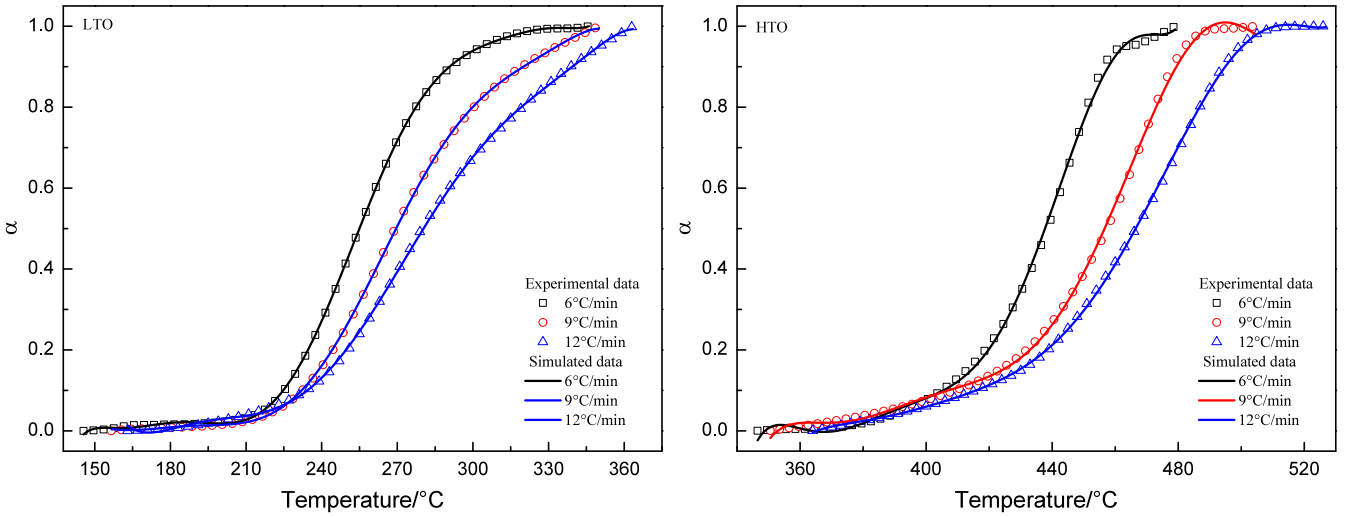

Figure 11. Comparison of specific $\alpha-T$ curves based on the experimental and simulated data.

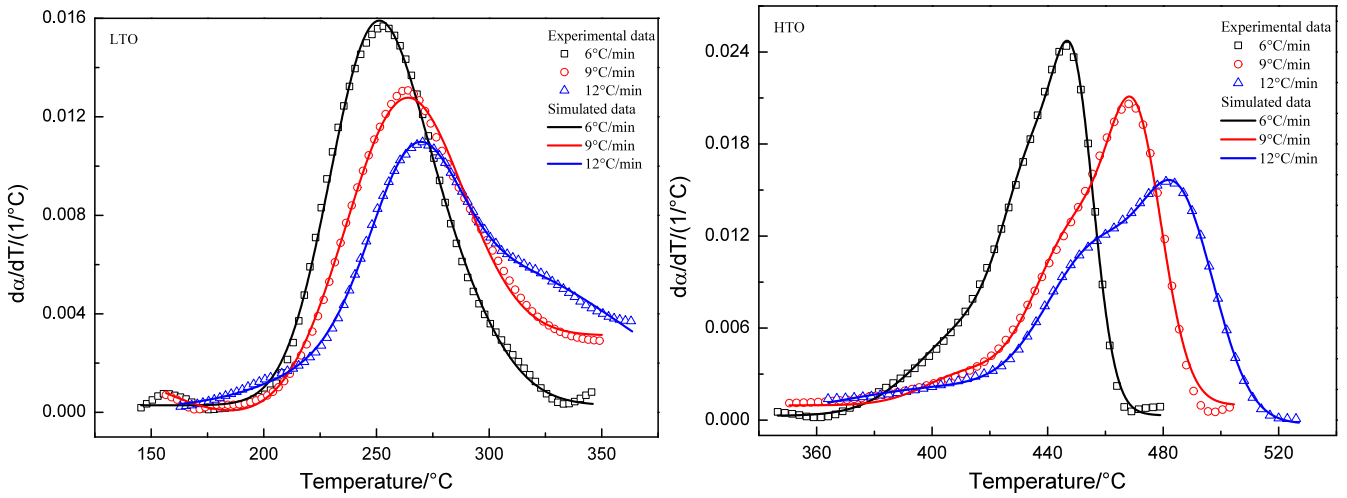

Figure 12. Comparison of specific $d\alpha/dT-T$ curves based on the experimental and simulated data.

corresponding to heating rates of 6, 9, and 12 °C/min, which were within the degree of tolerance and presented a satisfactory parallelism among experimental and simulated values. Therefore, the obtained kinetic triplet could be regarded as an important reference for subsequent numerical modeling to describe and predict oxidation behaviors during the ISC process, which kept in mind the change of kinetic parameters with conversion degree.

3.3. Evolution Pathway of the Ultraheavy Oil Combustion Process. As a mixture of hydrocarbons and related derivatives, complicated oxidation reactions for the heavy oil also followed a free radical mechanism during which the combustion behavior and kinetics were specific external manifestations. According to the above analyses and anterior studies, the evolution pathway of the ultraheavy oil during the oxidation process is proposed in Figure 13 to further understand the underlying LTO oxidation mechanism and dominant reaction pathway. As for the subsequent coke deposition and combustion process, related mechanism elucidation has been reported in previous studies.[5,7]

Based on the free radical theory,[32,33] the C−H bond in hydrocarbons (RH) was first attacked by the dissolved oxygen atoms to generate the alkyl free radical ($R^{\bullet}$), which was a signal

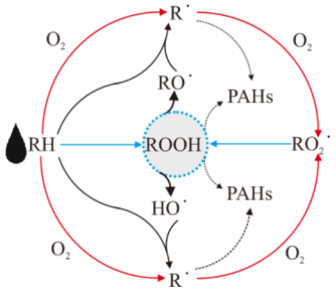

Figure 13. Schematic diagram of the free radical mechanism for the heavy oil oxidation process.

of the chain reaction initiation and the precondition for subsequent chain propagation and growth. Meanwhile, the formed $R^{\bullet}$ further reacted with oxygen atoms to generate the active peroxyalkyl radical ($RO_2^{\bullet}$) with certain heat release, as illustrated by the red pathway. As the intermediate propagated, part of the $RO_2^{\bullet}$ reacted with RH to obtain the LTO intermediate product (blue pathway), hydroperoxide (ROOH), which was unstable and easily decomposed into the alkoxy radical ($RO^{\bullet}$) and hydroxyl radical ($HO^{\bullet}$). In addition, decomposed products would react with surrounding RH to form

https://doi.org/10.1021/acsomega.4c01032
ACS Omega 2024, 9, 21164−21173

continuous $R^{\bullet}$ to accelerate the decomposition process and sustain the chain circulation (black pathway). Another $RO_2^{\bullet}$ would directly participate in the formation of a stable hydroperoxy radical ($HO_2^{\bullet}$) and the stable association of two $RO_2^{\bullet}$ radicals or $RO_2\bullet$ and $R^{\bullet}$ to weaken or terminate chain reactions, as shown by the dotted black pathway. It is worth noting that these pathways were interdependent rather than isolated, containing complicated addition, isomerization, aromatization, decomposition, and condensation reactions to form polycyclic aromatic hydrocarbons (PAHs).

4. CONCLUSION

This study comprehensively exhibited the characterization of nonisothermal combustion behaviors, determination of kinetic triplet variables, and evolution pathway of underlying oxidation reactions for the ultraheavy oil during the ISC process, and the following understandings are summarized as follows.

(1) Heating rate growth would worsen oxidation progress with a shift in the curve to the upper right. Furthermore, the comparison of DSC and PDSC curves indicated a positive signal and the possibility for a significant LTO exothermal increment under high-pressure reservoir conditions, subsequently promoting the combustion front stability.

(2) The LTO and HTO average activation energies via DAEM and Friedman methods were respectively determined and compared. Besides, the determined most probable mechanism functions were respectively the acceleratory rate model ($P_{-0.468}$) for LTO and the Sestak−Berggren ($S_{0.649}B_{0.886}$) model for HTO via the Shahcheraghi method. Moreover, there was a satisfactory match between experimental and calculated curves, implying that the attained kinetic triplet convincingly described and predicted the oxidation behaviors.

(3) For the LTO process, three primary evolution pathways were proposed to describe the underlying oxidation process. Meanwhile, complicated addition, isomerization, aromatization, decomposition, and condensation reactions were intertwined with each other to form polycyclic aromatic hydrocarbons (PAHs).

■ ASSOCIATED CONTENT

Supporting Information

The Supporting Information is available free of charge at https://pubs.acs.org/doi/10.1021/acsomega.4c01032.

Fundamental characterizations and several analysis materials for the heavy oil (PDF)

■ AUTHOR INFORMATION

Corresponding Author

Yafei Chen − *Engineering Research Center for Waste Oil Recovery Technology and Equipment, Ministry of Education, Chongqing Technology and Business University, Chongqing 400067, People's Republic of China;* orcid.org/0000-0003-4796-6438; Email: china_chenyf@163.com

Authors

Hong Yin − *Engineering Research Center for Waste Oil Recovery Technology and Equipment, Ministry of Education, Chongqing Technology and Business University, Chongqing 400067, People's Republic of China;* orcid.org/0000-0002-6353-1939

Ziqiang Chen − *Engineering Research Center for Waste Oil Recovery Technology and Equipment, Ministry of Education, Chongqing Technology and Business University, Chongqing 400067, People's Republic of China*

Hua Tan − *Engineering Research Center for Waste Oil Recovery Technology and Equipment, Ministry of Education, Chongqing Technology and Business University, Chongqing 400067, People's Republic of China*

Mingyuan Wang − *Sulige Project Management Department of CNPC Chuanqing Drilling Engineering Company Limited, Ordos, Inner Mongolia 017300, People's Republic of China*

Donglin He − *Engineering Research Center for Waste Oil Recovery Technology and Equipment, Ministry of Education, Chongqing Technology and Business University, Chongqing 400067, People's Republic of China;* orcid.org/0000-0003-3888-3040

Ping Ouyang − *Engineering Research Center for Waste Oil Recovery Technology and Equipment, Ministry of Education, Chongqing Technology and Business University, Chongqing 400067, People's Republic of China*

Haifeng Gong − *Engineering Research Center for Waste Oil Recovery Technology and Equipment, Ministry of Education, Chongqing Technology and Business University, Chongqing 400067, People's Republic of China*

Complete contact information is available at: https://pubs.acs.org/10.1021/acsomega.4c01032

Notes

The authors declare no competing financial interest.

■ ACKNOWLEDGMENTS

The authors wish to recognize the financial support received from the National Natural Science Foundation of China (No. 52300150), Chongqing Natural Science Foundation Project (CSTB2023NSCQ-MSX0834, CSTB2023NSCQ-MSX0737), Science and Technology Project of Chongqing Municipal Education Commission (KJQN202200841, KJQN202200812), Natural Science Innovation and Development Joint Foundation Project of CQCSTB (CSTB2023NSCQ-LZX0096), and Science and Technology Research Program of Chongqing Municipal Education Commission of China (KJZD-M202300802). In addition, the authors also thank the Northwest Oilfield Company, Sinopec (China), for providing the crude oil materials.

■ REFERENCES

(1) Hein, F. J.; Ambrose, W. A.; Hackley, P.; Mead, J. S. Unconventional energy resources: 2017 review. *Nat. Resour. Res.* **2019**, *28* (4), 1661−1751.

(2) Dudley, B. *BP statistical review of world energy*. BP Statistical Review: 2018.

(3) Mahinpey, N.; Ambalae, A.; Asghari, K. In situ combustion in enhanced oil recovery (EOR): A review. *Chem. Eng. Commun.* **2007**, *194* (8), 995−1021.

(4) Omoregbe, O.; Hart, A. Global Trends in heavy oil and bitumen recovery and in-situ ppgrading: A bibliometric analysis during 1900−2020 and future outlook. *J. Energy Resour. Technol.* **2022**, *144* (12), 123007−123018.

(5) Chen, Y. F.; Pu, W. F.; Liu, X. L.; Li, Y. B.; Varfolomeev, M. A.; Hui, J. A preliminary feasibility analysis of in situ combustion in a deep fractured-cave carbonate heavy oil reservoir. *J. Petrol. Sci. Eng.* **2019**, *174*, 446−455.

(6) Teng, L.; Song, H.; Zhang, S.; Wu, F.; Xu, D.; Gong, Y.; Jiang, Z.; Gao, H.; Wang, C.; Zhong, L. Investigation on in-situ combustion in

D66, a multilayered heavy oil reservoir, Liaohe Oilfield. *SPE 186173 presented at the SPE/IATMI Asia pacific oil & gas conference and exhibition*; Jakarta, Indonesia, October 17−19, 2017.
(7) Chen, Y. F.; Yin, H.; He, D. L.; Gong, H. F.; Liu, Z. Z.; Liu, Y. Q.; Zhang, X. M.; Pu, W. F. Low temperature oxidized coke of the ultra-heavy oil during in-situ combustion process: Structural characterization and evolution elucidation. *Fuel* **2022**, *313*, 122676−122686.
(8) Al Adasani, A.; Bai, B. Analysis of EOR projects and updated screening criteria. *J. Petrol. Sci. Eng.* **2011**, *79* (1−2), 10−24.
(9) Ahmadi Khoshooei, M.; Fazlollahi, F.; Maham, Y. A review on the application of differential scanning calorimetry (DSC) to petroleum products. *J. Therm. Anal. Calorim.* **2019**, *138* (5), 3455−3484.
(10) Kök, M. V. Recent developments in the application of thermal analysis techniques in fossil fuels. *J. Therm. Anal. Calorim.* **2008**, *91* (3), 763−773.
(11) Pu, W. F.; Chen, Y. F.; Li, Y. B.; Zou, P.; Li, D. Comparison of different kinetic models for heavy oil oxidation characteristic evaluation. *Energy Fuels* **2017**, *31* (11), 12665−12676.
(12) Vargas, J. A. V.; dos Santos, R. G.; Trevisan, O. V. Evaluation of crude oil oxidation by accelerating rate calorimetry. *J. Therm. Anal. Calorim.* **2013**, *113* (2), 897−908.
(13) Li, J.; Mehta, S.A.; Moore, R.G.; Zalewski, E.; Ursenbach, M.G.; Van Fraassen, K. Investigation of the oxidation behaviour of pure hydrocarbon components and crude oils utilizing PDSC thermal technique. *J. Can. Petrol. Technol.* **2006**, *45* (01), 48−53.
(14) Zhao, R.; Chen, Y.; Huan, R.; Castanier, L. M.; Kovscek, A. R. An experimental investigation of the in-situ combustion behavior of Karamay crude oil. *J. Petrol. Sci. Eng.* **2015**, *127*, 82−92.
(15) Jiang, H.; Zan, C.; Song, X. M.; Ma, D. S. Determination of oxidation kinetics parameters for crude oil using high pressure and near adiabatic calorimetry method. *Acta Petrolei Sinica* **2014**, *35* (4), 745−748.
(16) Vyazovkin, S.; Burnham, A. K.; Criado, J. M.; Pérez-Maqueda, L. A.; Popescu, C.; Sbirrazzuoli, N. ICTAC Kinetics Committee recommendations for performing kinetic computations on thermal analysis data. *Thermochim. Acta* **2011**, *520* (1−2), 1−19.
(17) Vyazovkin, S.; Burnham, A. K.; Favergeon, L.; Koga, N.; Moukhina, E.; Pérez-Maqueda, L. A.; Sbirrazzuoli, N. ICTAC Kinetics Committee recommendations for analysis of multi-step kinetics. *Thermochim. Acta* **2020**, *689*, 178597−178618.
(18) Kök, M. V.; Acar, C. Kinetics of crude oil combustion. *J. Therm. Anal. Calorim.* **2006**, *83* (2), 445−449.
(19) Chen, Y. F.; Pu, W. F.; Liu, X. L.; Li, Y. B.; Gong, X. L.; Hui, J.; Guo, C. Specific kinetic triplet estimation of Tahe heavy oil oxidation reaction based on non-isothermal kinetic results. *Fuel* **2019**, *242*, 545−552.
(20) Shahcheraghi, S. H.; Khayati, G. R.; Ranjbar, M. An advanced reaction model determination methodology in solid-state kinetics based on Arrhenius parameters variation. *J. Therm. Anal. Calorim.* **2015**, *122* (1), 175−188.
(21) Chen, Y. F.; Pu, W. F.; Li, Y. B.; Liu, X. L.; Jin, F. Y.; Hui, J.; Gong, X. L.; Guo, C. Novel insight into the viscosity-temperature characteristic by the comparison of Tahe ordinary-and ultra-heavy oils. *Energy Fuels* **2018**, *32* (12), 12308−12318.
(22) ASTM, D., *Standard Method of Preparing Coal Samples for Analysis*; American Society for Testing and Materials: 2013.
(23) Chen, Y. F.; Liu, Z. Z.; Wang, M. Y.; Yin, H.; He, D. L.; Gong, H. F.; Zhang, X. M. New insights into the non-isothermal oxidation of tight oil: Experimental study and theoretical prediction. *Fuel* **2022**, *326*, 125011−125019.
(24) Dunn, R. O. Oxidative stability of biodiesel by dynamic mode pressurized-differential scanning calorimetry (P-DSC). *T. ASABE* **2006**, *49* (5), 1633−1641.
(25) Elder, J. P. The E-ln(A)-f(α)' triplet in non-isothermal reaction kinetics analysis. *Thermochim. Acta* **1998**, *318* (1−2), 229−238.
(26) Xu, D. P.; Chen, Y. F.; Wu, Y.; Wang, Y. Sorption of mercury (II) and arsenic (III) on humic acid from peatsoil. *Chin. J. Environ. Eng.* **2017**, *11* (9), 5275−5282.
(27) Miller, J. A.; Sivaramakrishnan, R.; Tao, Y.; Goldsmith, C. F.; Burke, M. P.; Jasper, A. W.; Hansen, N.; Labbe, N. J.; Glarborg, P.; Zádor, J. Combustion chemistry in the twenty-first century: Developing theory-informed chemical kinetics models. *Prog. Energy Combust.* **2021**, *83*, 100886−100939.
(28) Shahcheraghi, S. H.; Khayati, G. R.; Ranjbar, M. An advanced reaction model determination methodology in solid-state kinetics based on Arrhenius parameters variation. *J. Therm. Anal. Calorim.* **2016**, *126* (2), 981−993.
(29) Vyazovkin, S. *Isoconversional kinetics of thermally stimulated processes*; Springer: 2015.
(30) Eyring, H. The activated complex and the absolute rate of chemical reactions. *Chem. Rev.* **1935**, *17* (1), 65−77.
(31) Wu, W.; Cai, J.; Liu, R. Isoconversional kinetic analysis of distributed activation energy model processes for pyrolysis of solid fuels. *Ind. Eng. Chem. Res.* **2013**, *52* (40), 14376−14383.
(32) Freitag, N. P. Chemical-reaction mechanisms that govern oxidation rates during in-situ combustion and high-pressure air injection. *SPE Reserv. Eval. Eng.* **2016**, *19* (04), 645−654.
(33) Sahoo, A.; Gautam, R.; Kumar, S.; Mohanty, K. Energy optimization from a binary mixture of non-edible oilseeds pyrolysis: Kinetic triplets analysis using Thermogravimetric Analyser and prediction modeling by Artificial Neural Network. *J. Environ. Manage.* **2021**, *297*, 113253−113266.

https://doi.org/10.1021/acsomega.4c01032
ACS Omega 2024, 9, 21164−21173